



# Producing high quality biofuels: Pt-based hydroisomerization catalysts evaluated using BtL-naphtha surrogates

Eleni F. Iliopoulou\*, Eleni Heracleous, Andreas Delimitis, Aggelos A. Lappas

Chemical Process Engineering Research Institute (CPERI), Centre for Research and Technology Hellas (CERTH), P.O. Box 60361, GR-57001 Thessaloniki, Greece



## ARTICLE INFO

### Article history:

Received 19 December 2012

Received in revised form 8 March 2013

Accepted 12 March 2013

Available online 23 March 2013

### Keywords:

BtL naphtha

Hydroisomerization

Pt

Mordenite

ZSM-5

Beta zeolite supports

Acidity

HR-TEM

## ABSTRACT

A series of low loading, platinum-containing catalysts was successfully synthesized impregnating three different acid zeolitic supports of similar  $\text{SiO}_2/\text{Al}_2\text{O}_3$  ratio (~20) but various structure and acidic characteristics (mordenite, ZSM-5, BETA) with an aqueous  $\text{H}_2\text{PtCl}_6$  solution. All catalysts were thoroughly characterized (ICP, XRD,  $\text{N}_2$  physisorption, FTIR–pyridine adsorption and HR-TEM) and studied as candidate hydroisomerization catalysts. In order to accomplish the above purpose, the Pt-loaded zeolites were tested using surrogate naphtha feeds focusing on the effect of the zeolite support, as well as the nature of the feed (additionally examining heavier feeds (>C6), such as BtL-naphtha) on the activity and selectivity of the catalysts. Both Pt/MOR and Pt/ZSM-5 materials contain large numbers of total and Brønsted acidity. However, Pt/ZSM-5 slightly prevails over Pt/MOR concerning acidity strength; thus exhibiting the highest catalytic activity (highest conversion). The same Pt/ZSM-5 catalyst was also able to successfully isomerize heavier hydrocarbons with limited cracking side reactions. Besides acidity, the efficiency of Pt/ZSM-5 is possibly attributed to the faster mobility of carbocation intermediates through its more interconnected structure and the formation of homogeneously dispersed, cubic-shaped and highly crystalline Pt particles along with highly dispersed Pt species on the zeolite surface.

© 2013 Elsevier B.V. All rights reserved.

## 1. Introduction

The Biomass-to-Liquids (BtL) process, which involves the gasification of lignocellulosic biomass to syngas and its conversion to hydrocarbons via Fischer–Tropsch, constitutes one of the most promising technologies for the production of high quality 2nd generation biodiesel fuels. Although the light by-product of FT-synthesis is not a suitable fuel for conventional engines, BtL-naphtha has the potential to become the best suited fuel for future power-trains like HCCI (Homogeneous Charge Compression Ignition). Preliminary tests however indicated that further upgrading of the naphtha fraction is needed for optimized engine performance, targeted toward mild reduction of its cetane number [1], which can be achieved via hydroisomerization of BtL-naphtha.

Hydroisomerization is a very important catalytic process in the petroleum industry, which converts linear alkanes to their corresponding branched isomers. Hydroisomerization of C4–C7 hydrocarbons is applied for the production of gasoline with a high octane number, while isomerization of C7–C15 paraffins is employed for the production of diesel fuel with improved cold

flow properties, such as viscosity, pour point and freezing point [2]. Several variables, including operating conditions such as reaction temperature, contact time, pressure and  $\text{H}_2$ /hydrocarbon ratio [3] as well as catalytic properties, like the distribution of metal and acid sites [4,5] play an important role in this process and have been extensively studied [3–5].

Isomerization requires bifunctional catalysts, containing both metallic sites for hydrogenation/dehydrogenation and acidic sites for the skeletal re-arrangement via carbenium ions reactions, respectively. The isomerization reaction proceeds via the dehydrogenation of alkanes on the metallic sites, while the produced olefins are protonated on the Brønsted acid sites to the corresponding alkylcarbenium ions. These carbenium ions can undergo skeletal rearrangement and b-scission, followed by de-protonation and hydrogenation over metal sites to produce the isomerization and cracking products. During this mechanistic pathway, it is very important to minimize the secondary reactions and to ensure a satisfactory reaction rate. To achieve this, it is necessary to have a defined ratio between the metal and acid sites [6]. Lin, Zhang and Liang [7–9] showed that the higher the acidity of the support, the more enhanced are the cracking reactions at the expense of the selectivity to hydroisomerization. They also suggest that metal sites and catalyst support interact forming a “hybrid” active site, which seems to enhance the hydrogenation activity constraining undesired cracking reactions.

\* Corresponding author. Tel.: +30 2310 498312; fax: +30 2310 498380.

E-mail address: [eh@cpri.certh.gr](mailto:eh@cpri.certh.gr) (E.F. Iliopoulou).

Currently the industrial catalysts are Pt-based supported either on chlorinated alumina or zeolites, mainly mordenites, and are designed for the isomerization of light feeds ( $C_5/C_6$ ) [10]. Catalysts supported on chlorinated alumina are highly active at low temperatures ( $130^\circ\text{C}$ ), but suffer from extreme sensitivity to feed contaminants, such as water and sulfur traces ( $<0.5\text{ ppm}$  and  $<0.1\text{ ppm}$ ), which poison the catalyst and lower its activity. Furthermore, the pressure of the hydrogen in the reactor results in the elution of chlorine from the catalyst as hydrogen chloride, causing corrosion problems. Finally, the catalysts must be activated, periodically injecting  $\text{CCl}_4$  or  $\text{C}_2\text{Cl}_4$  in the feed [11–13].

Zeolite-supported catalysts although less active, are characterized by their outstanding tolerance to feed poisons (sulfur and water) and therefore do not require feed pretreatment. Moreover, they are more resistant to the presence of aromatics, while they simultaneously have the advantage of a well-defined porous structure, which allows one to select the most suitable structure for the process [6]. However, zeolite-based catalysts exhibit lower activity and thus the reaction must be performed at higher temperatures ( $250^\circ\text{C}$ ), favoring unwanted cracking side reactions [2,14]. Great efforts have been directed to modify zeolite supports in these catalysts via strengthening or creating stronger acid sites, compared to the traditionally used-alumina support, as well as modifying the metal sites via incorporating metallic promoters [14–16].

It is noteworthy that longer n-alkanes are more easily converted to isoalkanes and/or cracked alkanes than shorter n-alkanes. Unfortunately, multibranched alkanes are susceptible to hydrocracking. If the pore size is made small enough to restrain multibranched isoalkanes from being further converted at inner acidic sites, the isomerization selectivity can be increased. Therefore, shape selectivity of zeolites is probably their most significant and advantageous property, which can be used to suppress the formation of multibranched isoalkanes and thus inhibit hydrocracking reactions, finally improving isomerization selectivity [17,18]. When referring to shape selectivity, we address the fact that the hydroisomerization performance of a zeolite depends on several parameters such as the zeolite topology, pore size, window size and dimensionality of the pore system. For example, it is reported that the methyl branching is favored with small pore zeolites and that the ethyl and/or propyl branchings are favored with wide pore openings and large cavities [19].

An additional approach toward improved catalytic performance is to use catalysts either with weak acidity for suppressing the hydrocracking of multibranched alkylcarbenium ions or with high metal dispersion for enhancing the hydrogenation of desorbed multibranched alkenes [19]. The balance between the two catalytic functions, i.e. the density and the strength of the Brønsted acid sites ( $\text{H}^+$ ) and the amount and the dispersion of the metal [20–25] is what determines the desired selectivity. When the hydrogenating function is highly active, the activity and the selectivity of the bifunctional catalyst will depend only on the acidic function, which is the rate-limiting step in the absence of diffusion limitations. A decrease in acidity would decrease cracking [19,26], but also the global activity since the acidic step is rate-limiting [19,27]. Metal content in the hydroisomerization catalysts has also a crucial effect on the catalytic activity and selectivity [28–31]. However, the optimum Pt content in the majority of modern industrial light naphtha hydroisomerization catalysts is in the range of 0.40% [11].

Summarizing all above, an ideal hydroisomerization catalyst should provide a high yield of isomerization and should have shape-selectivity to react only with n-paraffins. To achieve these characteristics, the catalyst should have suitable compositional and structural characteristics, mainly: proper balance between metal and acid sites, medium pore size, high dispersion of metal on the catalyst surface, mild acidity and strength distribution of acid sites [2]. Thus, for a well balanced (with a strong hydrogenating

function) catalyst the product distribution will depend essentially on its acidic properties and its pore structure [32,33]. Finally, the step of chemical transports of intermediates between sites is of the greatest importance [34–36].

Aim of the current work is the study and development of Pt-based hydroisomerization catalysts supported on various zeolitic carriers (ZSM-5, mordenite and beta zeolite). The effect of zeolite support on the activity and selectivity of the catalysts in naphtha hydroisomerization is discussed in view of detailed physicochemical characterization of the materials, aiming to correlate acidic and shape selectivity characteristics to the differentiating hydroisomerization activity and selectivity. The same Pt/zeolite catalysts were also tested for the isomerization of heavier feeds ( $>\text{C}_6$ ), such as BtL-naphtha. As the selective isomerization of heavy n-alkanes is much more difficult due to the rapid cracking of long chain alkanes, the investigation focused on developing catalytic systems with high selectivity to isomerization rather than cracking. Thus, results are also presented on the effect of the nature of the feed (aromaticity, heaviness), investigated with experiments conducted with surrogate naphtha feeds.

## 2. Experimental part

### 2.1. Catalyst preparation

Three different commercial zeolites (mordenite: MOR, BETA and ZSM-5) with similar  $\text{SiO}_2/\text{Al}_2\text{O}_3$  ratio ( $\sim 20$ ) were used as supports. All zeolites [MOR(20), ZSM-5(23), BETA(25), where the numbers in brackets denote the respective  $\text{SiO}_2/\text{Al}_2\text{O}_3$  ratio] were purchased from Zeolyst Int. (refs. CBV21A, CBV2314 and CP814E, respectively). The supports were calcined in air at  $500^\circ\text{C}$  for 3 h prior to impregnation to convert from the ammonium to the  $\text{H}^+$ -form. Impregnation followed using an aqueous solution of  $\text{H}_2\text{PtCl}_6$  in order to achieve a 0.1 wt% Pt loading on the final material. Excess distilled water was used as solvent for this precursor. The derived catalysts were dried and calcined at  $400^\circ\text{C}$  for 3 h under air using a synthetic air stream.

### 2.2. Catalyst characterization

The elemental composition (Al, Na and Pt content) of all samples was measured by inductively coupled plasma-atomic emission spectroscopy (ICP-AES) with a Perkin-Elmer Plasma 40 instrument.

X-ray diffraction (XRD) measurements were also performed using a SIEMENS D-500 diffractometer employing  $\text{CuK}\alpha_1$  radiation ( $\lambda = 0.15405\text{ nm}$ ) and operating at 40 kV and 30 mA. The XRD patterns were accumulated in the  $2\theta$  range of  $5\text{--}80^\circ$  with a  $0.02^\circ$  step size and a counting time of 2 s per step.

Surface areas of the samples were determined by  $\text{N}_2$  adsorption at  $77\text{ K}$ , using the multipoint BET analysis method, with an Autosorb-1 Quantachrome flow apparatus. Prior to the measurements, the samples were dehydrated in vacuum at  $250^\circ\text{C}$  overnight. The Brunauer–Emmet–Teller (BET) equation was used to calculate the apparent surface area (SBET), while the micropore volume ( $V_{\text{micro}}$ ) and the external surface (Sext) were calculated from t-plot method.

To examine the tendency of catalyst to form coke (related with hydrocracking reactions) C content was determined by elemental analysis using a LECO-800 CHN analyzer on all catalytic samples; Pt/MOR(20), Pt/ZSM-5(23) and Pt/BETA(25) after the hydroisomerization reaction.

The total acidity, type and acid strength distribution of the acid zeolites were measured by the FTIR-pyridine adsorption technique. IR spectra were collected using a Nicolet 5700 FTIR spectrometer (resolution  $4\text{ cm}^{-1}$ ) by means of OMNIC software. Data processing was carried out via the GRAMS software. All the samples were

**Table 1**  
Properties and composition of the tested naphtha surrogate feeds.

Feed	Light – A	Heavy – B
Density, g/cm <sup>3</sup>	0.67	0.69
Cetane index	34.2	50.4
<i>Composition, wt%</i>		
C5 normal paraffin	35.48	4.94
C6 normal paraffin	42.32	12.05
C7 normal paraffin	3.45	15.33
C8 normal paraffin		15.65
C9 normal paraffin		11.71
C10 normal paraffin		5.98
C5 iso paraffin	0.73	3.08
C6 iso paraffin	0.04	6.21
C7 iso paraffin	2.12	
C8 iso paraffin		25.04
C6 saturated naphthene	10.03	
C6 aromatic	5.71	

finely ground in a mortar and pressed in self-supporting wafers ( $\sim 15 \text{ mg/cm}^2$ ). The wafers were placed in a homemade stainless steel, vacuum cell, with  $\text{CaF}_2$  windows. High vacuum was reached by the means of a turbomolecular pump and a diaphragm pump placed in line. The infrared cell was equipped with a sample holder surrounded by a heating wire for the heating steps and connected to the vacuum line, which is also heated in order to avoid pyridine condensation or its adsorption on the walls. Before IR analysis, all samples were heated at  $450^\circ\text{C}$  under high vacuum ( $10^{-6} \text{ mbar}$ ) for 1 h in order to desorb any possible physisorbed species (activation step). All spectra were collected at  $150^\circ\text{C}$  in order to eliminate the possibility of pyridine condensation. Initially, the reference spectrum of the so-called activated sample is collected. Then adsorption of pyridine is realized at 1 mbar by equilibrating the catalyst wafer with the probe vapour, added in pulses for 1 h. The desorption procedure of pyridine is stepwisely monitored by evacuating the sample for 30 min at 150, 250, 350 and  $450^\circ\text{C}$  and cooling down to  $150^\circ\text{C}$  after each step to record the corresponding spectrum.

In-depth characterization of the materials was also performed with conventional as well as high resolution transmission electron microscopy (TEM-HRTEM). Samples for electron microscopy observations were prepared by gently grinding the catalyst powders in high-purity ethanol using an agate pestle and mortar. A drop of the solution was subsequently deposited onto a lacey C-film supported on a Cu grid and allowed to evaporate under ambience conditions. Electron microscopy experiments were carried out in a JEOL 2011 high resolution transmission electron microscope, operating at 200 kV, with a point resolution of 0.23 nm and  $C_s = 1.0 \text{ mm}$ . Chemical analysis of the catalysts is carried out by the energy-dispersive X-ray spectroscopy (EDS) technique. For this reason, the microscope is fitted with an Oxford Instruments INCAx-sight liquid nitrogen cooled EDS detector with an Si(Li) window. Processing of the spectra was accomplished using the INCA Microanalysis Suite software.

### 2.3. Feedstocks

In order to investigate the effect of the composition of the naphtha feedstock, the isomerization tests were conducted with two different surrogate naphtha feeds prepared in the lab using chemical grade reagents: light feed A (C5–C7) and heavy feed B (C5–C10). The main properties and the chemical composition of the investigated feeds are tabulated in Table 1. The cetane index (CI) of the feeds is also reported. As there is no commercially available software for CI estimation on naphthas, the estimation was performed with a method developed in CPERI, based on the individual volumetric contribution of each hydrocarbon in the feed. The same

**Table 2**  
Chemical composition of zeolitic supports and Pt/zeolite catalysts.

Catalyst	Al (wt%)	Na (wt%)	Pt (ppm)	
			Nominal loading	Actual loading
H-MOR(20)	$3.30 \pm 0.16$	0.0125	–	–
Pt/MOR(20)	$3.25 \pm 0.16$	0.0120	1000	$1350 \pm 90$
H-ZSM-5(23)	$2.915 \pm 0.14$	0.0650	–	–
Pt/ZSM-5(23)	$2.91 \pm 0.14$	0.0640	1000	$1095 \pm 65$
H-BETA(25)	$2.64 \pm 0.13$	0.0150	–	–
Pt/BETA(25)	$2.65 \pm 0.13$	0.0140	1000	$1115 \pm 80$

method was used for the estimation of the CI of the isomerization products presented in the results.

### 2.4. Isomerization tests

The hydroisomerization tests were performed on a high pressure small scale test unit of CPERI, a newly constructed versatile unit for the evaluation of the activity and selectivity of solid catalytic materials in different high pressure reactions. The unit is equipped with a feed inflow system able to supply both gases and liquid feeds. There are three gas lines, controlled by high accuracy mass flow controllers and one liquid feed line, delivering liquid hydrocarbon feedstocks via a high precision pump. The unit operates with a stainless steel fixed bed reactor (ID: 9.3 mm), externally heated with a three-zone furnace, while the exit stream of the reactor is cooled via a heat exchanger and is directed to a system of vessels for the separation and collection of the liquid and gaseous products. The reaction temperature is monitored with a thermocouple inserted in the catalytic bed. Both the liquid products and the gaseous stream are analyzed with gas chromatographs. The test facility can operate to a temperature range up to  $600^\circ\text{C}$  and pressures up to 100 atm.

The isomerization tests were performed in the stainless steel fixed bed reactor loaded with appropriate amount of the crushed catalyst. Prior to the measurements, the catalyst was stabilized submitting it to a pretreatment under a flow of  $\text{H}_2$  and naphtha feed. The reaction was conducted at 30 bar, using a weight hourly space velocity (WHSV) of  $2 \text{ h}^{-1}$ . The reaction temperature was varied from 240 to  $300^\circ\text{C}$ . Steady-state activity measurements were taken after at least 8 h on-stream, collecting and analyzing both a liquid and a gaseous product sample. The liquid samples were analyzed with PIANO analysis (hydrocarbon analysis carried out by GC to determine the amount of paraffin (P), isoparaffins (I), aromatics (A), naphthalene (N), and olefins (O)), while the composition of the reaction off-gases was detected with a GC.

## 3. Results

### 3.1. Catalyst characterization

#### 3.1.1. Elemental Composition and crystallinity of zeolite based catalysts

The elemental composition (Al, Na and Pt content) of all zeolitic supports and Pt/zeolite catalysts are presented in Table 2. The ZSM-5 supported material is the one with the smallest difference between nominal and actual metal loading and the lowest Pt content. The MOR supported sample is the one with the highest Pt loading, thus potentially expected to exhibit an increased hydrogenation activity and an enhanced performance.

As checked by using the X-ray diffraction technique all zeolites (mordenite, ZSM-5 and BETA) preserved their initial structure upon deposition of the metal and calcination treatment after impregnation. This was normally expected, due to the rather low metal loading (0.1% Pt) incorporated in the zeolitic supports.

**Table 3**

Porosity characteristics of zeolitic supports and Pt/zeolite catalysts.

Catalyst	Support	Zeolite surface area (m <sup>2</sup> /g)	Zeolite microporosity (cm <sup>3</sup> /g)
H-MOR(20)	–	528.42	0.1904
Pt/MOR(20)	H-MOR(20)	523.27	0.1813
H-ZSM-5(23)	–	417.69	0.1429
Pt/ZSM-5(23)	H-ZSM-5(23)	415.53	0.1211
H-BETA(25)	–	671.42	0.1820
Pt/BETA(25)	H-BETA(25)	654.28	0.1745

### 3.1.2. Porosity characteristics

Both selectivity and activity depend on the pore structure of zeolites, as porosity affects accessibility to the acid sites. Another factor that influences selectivity is the diffusion of the formed product species to the zeolite outer surface [36]. The three zeolites used in the present work have very different pore systems [37]:

- Mordenite is considered to have a monodimensional pore system with pore dimensions 6.2 Å × 7.2 Å.
- ZSM-5 has straight channels (5.6 Å × 5.6 Å) interconnected through sinusoidal channels (5.5 Å × 5.6 Å). The channels intersections generate 8.5 Å cavities.
- BETA has straight channels (7.6 Å × 6.4 Å) interconnected through sinusoidal channels (diameter 5.6 Å). The channels intersections generate 12–13 Å cavities [27].

As a consequence, the acidic sites in the larger pore systems (mordenite and BETA) are expected to be much more accessible to the n-alkane than the acidic sites in ZSM-5 supported catalysts.

All zeolitic supports used had a high specific surface area, which is typical of these materials (Table 3). Impregnation with the platinum salt scarcely altered area values; thus, catalysts Pt/MOR(20), Pt/ZSM-5(23) and Pt/BETA(25) still had a high specific surface area in agreement with values found in the literature [38].

### 3.1.3. Acidic properties

As already underlined, the acidity of the catalyst has a major effect on the hydroisomerization and hydrocracking reactions involved in our process. The density and strength of acidic sites are important, and an adequate balance between these parameters is critical to reactivity and selectivity. In general, catalysts with high hydrogenation ability and low acidity are desirable for the hydroisomerization of long chain hydrocarbons [19,23].

The acidic characteristics (total acidity and type of acids sites) of all zeolitic supports and Pt-based catalysts are summarized in Table 4. As evidenced from the initial comparison among the zeolitic supports, MOR and ZSM-5 exhibit a rather similar total acidity, while the acidity of BETA zeolite is more than 40% lower. Acidity is expected to decrease with increasing Si/Al ratio, in consistence with a decrease in the number of Si—O(H)—Al groups. However, in this case, small differences in SiO<sub>2</sub>/Al<sub>2</sub>O<sub>3</sub> among the supports tested cannot account for their differentiating acidity, which also depends on the different zeolite structure. In addition hydrothermal stability of each type of zeolite to the self-steaming effect during the initial

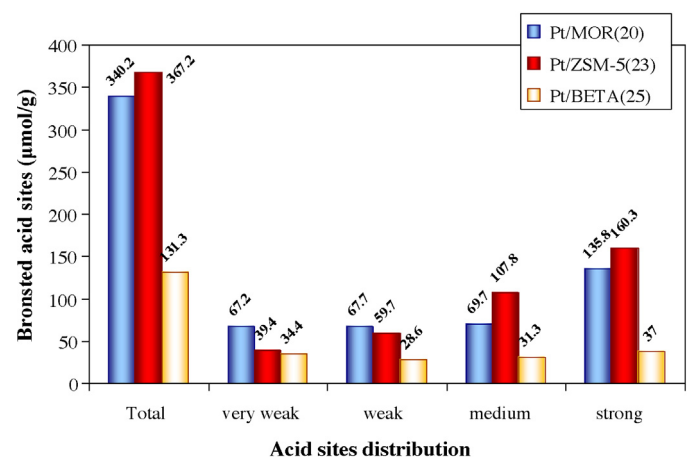


**Fig. 1.** Total Brønsted acidity and strength distribution of Brønsted acid sites of Pt/zeolite catalysts.

calcination treatment in order to convert the ammonium to the H<sup>+</sup>-form can vary significantly. It seems that BETA(25) is not so stable to this treatment leading to the formation of extra framework aluminum species, as additionally evidenced by the higher Lewis acidity. This might be a serious drawback considering commercial use of this catalyst which would require its periodical regeneration to remove coke depositions. Moreover, the percentage of Brønsted acid sites is ~83%, ~81% and ~43% of the total acidity for the zeolites MOR(20), ZSM-5(23) and BETA(25), respectively. As shown in Table 4, Pt deposition and the successive calcination step significantly decreased total acidity (mainly lowering Brønsted sites) of all zeolitic supports. The ZSM-5(23) exhibited the highest decrease (~23.1%) in Brønsted acidity followed by MOR(20) and BETA(25) (suffered from ~20.1% and 11.3% decrease, respectively). A similar ranking was observed on the loss of total acidity. However, still the Pt/ZSM-5 and Pt/MOR were those containing the largest numbers of total and Brønsted acidity, while Pt/BETA possesses the smallest, in accordance to literature results [38].

The strength distribution of the Brønsted acid sites on the Pt/zeolite catalysts is illustrated in Fig. 1. Once more the Pt/ZSM-5 prevails, as it possesses the highest proportion of strong sites (43.7% of total acidity) as compared with 39.9% for Pt/MOR and 28.2% for Pt/BETA respectively in agreement with previous work [38]. Finally, in combination with the porosity characteristics; i.e. surface area (Table 3) HZSM-5 zeolite acquires the higher density of strong acid sites. This is in agreement with the work of Aboul-Gheit [14], who however suggests that strong acid sites in H-ZSM-5 are still somewhat weaker than the respective sites in H-MOR. Moreover, these supposed to be milder sites in H-ZSM-5 zeolite were reported to enhance hydroisomerization and dehydrocyclization but suppress hydrocracking after incorporating 0.15% Pt.

### 3.1.4. Electron microscopy analysis

Two typical TEM images from the Pt/ZSM-5 catalyst are presented in Figs. 2(a) and 3(a). The zeolite comprises of large rectangular platelets, with sizes up to 900 nm and a high degree of crystallinity. This is better illustrated in the inset (b) of Fig. 2, where the (101) and (020) crystal planes of the orthorhombic ZSM-5 structure are observed, having an interplanar distance of  $d_{101} = 1.106$  nm and  $d_{020} = 0.985$  nm, respectively. On top of such platelets, smaller Pt nanoparticles – black-arrowed in Figs. 2(a) and 3(a) – are randomly distributed. The Pt particles have sizes up to 15 nm and characteristic cubic shape that demonstrates their single crystalline state and fcc Pt structure. Their detailed structural features are best depicted in the inset (b) of Fig. 3, where an HRTEM image of a Pt nanoparticle, at the edge of the ZSM-5

**Table 4**

Acidic properties of zeolitic supports and Pt/zeolite catalysts.

Catalyst	Brønsted sites (μmol/g)	Lewis sites (μmol/g)	Total acidity (μmol/g)
H-MOR(20)	428.8	88.3	517.1
Pt/MOR(20)	340.2	79.8	420.0
H-ZSM-5(23)	477.4	113.4	590.8
Pt/ZSM-5(23)	367.2	86.4	453.6
H-BETA(25)	148.1	198.7	346.8
Pt/BETA(25)	131.3	178.7	310.0

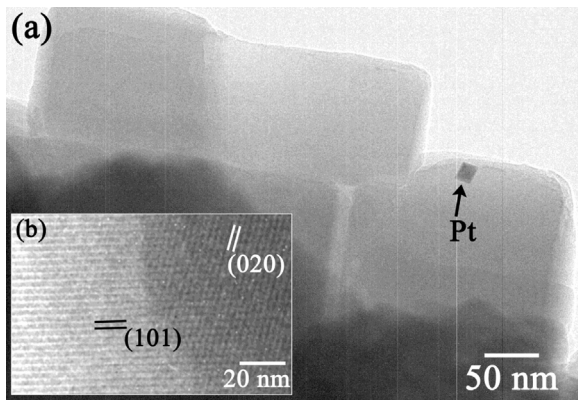


**Fig. 2.** (a) Representative TEM image of ZSM-5 platelets in the Pt/ZSM-5 catalyst. The position of a Pt single crystalline particle is black arrowed. (b) HRTEM image from the edge of a ZSM-5 platelet, predominately revealing (101) and (020) lattice fringes.

platelet is shown. The particle is oriented along its [110] zone axis and the two sets of {111}- and {111}-type lattice fringes with spacing  $d_{111} = 0.225$  nm are revealed. The termination of lattice planes almost up to its free surface clearly denotes the perfect crystal structure, with only a tiny outermost layer to be slightly disordered. EDS analysis revealed the existence of solely Pt and no other impurities. Some other smaller Pt particles with no specific shape were also dispersed onto the ZSM-5 platelets, but they comprise only a small fraction of the catalyst.

**Fig. 4(a)** shows a TEM image of the Pt/MOR catalyst. The mordenite platelets are randomly stacked, have sizes up to 350–400 nm and no specific shape. They are single crystalline, as better illustrated in the HRTEM image of inset (b), where the  $B = [001]$  projection of mordenite is shown [also depicted in the Fourier transform of **Fig. 4(c)**]. The main sets of fringes resolved correspond to the (110), (110) and (020) and (200) lattice planes, with a separation of  $d_{110} = 1.375$  nm,  $d_{020} = 1.011$  nm and  $d_{200} = 0.931$  nm, respectively. Pt particles are readily observed on top of the mordenite platelets, often with no specific shape and sizes ranging from 5 nm up to 25–28 nm. The Pt particles, although larger than those at the Pt/ZSM-5 catalyst are, to an extent, less crystalline. This is verified both by their random shape and the electron diffraction experiments performed on them; in addition, this was implied by the EDS analysis, where regions with trace amounts of impurities, such as Cl, were detected, too. It should be also pointed out that Pt particles are more unevenly distributed on the surface of the mordenite platelets compared to these at Pt/ZSM-5.

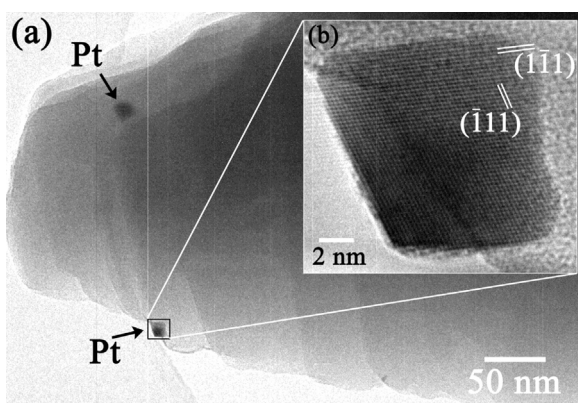


**Fig. 3.** (a) TEM image depicting the dispersion of the Pt particles on the ZSM-5 platelets and (b) typical HRTEM image of a single crystalline Pt particle, oriented along its [110] zone axis.

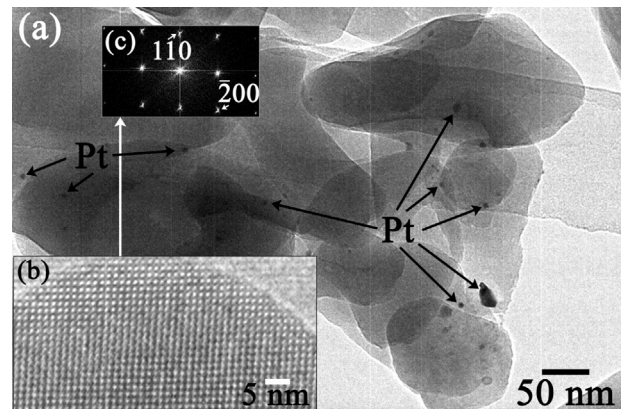


**Fig. 4.** (a) TEM image from the Pt/MOR catalyst, where the morphology of the mordenite and Pt and the metal dispersion are both revealed. The crystal quality of the zeolite is presented in the HRTEM image and the corresponding FT in (b) and (c), respectively, where the mordenite [001] projection is shown.

TEM characterization of the Pt/BETA zeolite sample revealed a distinct morphology for the zeolite particles, as depicted in **Fig. 5(a)**. The beta zeolite particles have quite small sizes, 10–20 nm and adopt a densely agglomerated morphology. The primary zeolite particles are single crystalline, as proved in the HRTEM image of **Fig. 5(b)**, where two sets of {101}-type lattice fringes, with  $d_{101} = 1.13$  nm are predominately resolved. Pt presence in this catalyst at discrete nanoparticle morphology was not observed by TEM or HRTEM imaging experiments. The random stacking of the beta particles, which may have hindered any Pt ones, is an additional drawback. Only by means of EDS was the detection of Pt possible, in areas such as the one presented in **Fig. 5(a)**. Trace amounts of Cl, were also found in the EDS spectra acquired from such areas, which was slightly higher among the three catalysts studied.

### 3.2. Catalytic performance

#### 3.2.1. Effect of zeolite support

The effect of zeolite support (ZSM-5, mordenite and beta zeolite) on the activity and selectivity of the catalysts in naphtha hydroisomerization was investigated by performing bench scale experiments at constant pressure, weight hourly space velocity, H<sub>2</sub>/HC molar ratio of 0.4 and varying temperature in the range of 240–300 °C. The initial hydroisomerization measurements were conducted with the light A surrogate naphtha feed, which consists mainly of C<sub>5</sub>–C<sub>7</sub> hydrocarbons. The atmosphere of hydrogen is expected to minimize carbon deposits on the catalyst. Analysis

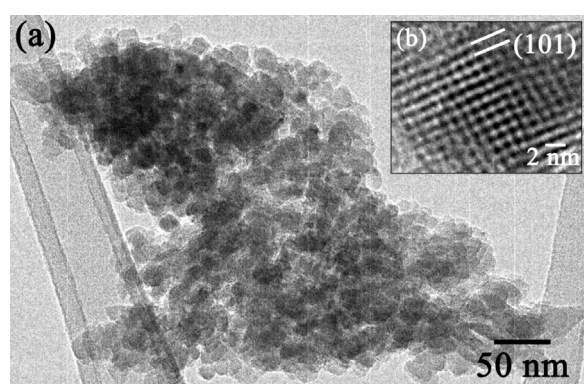


**Fig. 5.** (a) TEM image from the Pt/BETA catalyst showing the morphology and dense agglomeration of the beta particles. Their crystal quality is depicted in the HRTEM image in (b), where the {101}-type lattice fringes are predominately resolved.

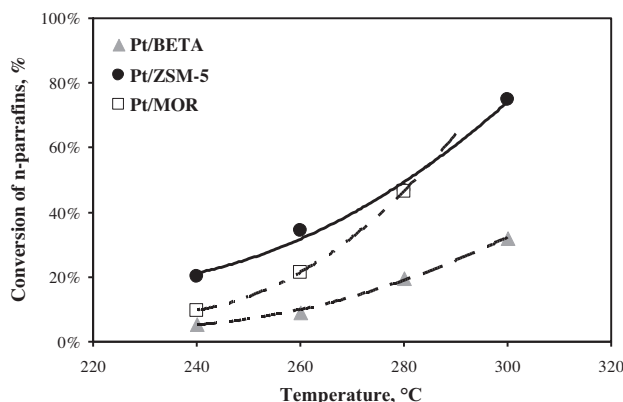


**Fig. 6.** Conversion of n-paraffins as a function of reaction temperature using as feed surrogate light naphtha A (reaction conditions:  $P=30$  bar,  $WHSV=2\text{ h}^{-1}$ ).

of the gases exiting the reactor with GC showed that hydrogen consumption is negligible, in accordance with literature [6]. With the employed Pt/zeolite catalysts, hydroisomerization is expected to take place via bifunctionality: Pt sites perform the hydrogenation–dehydrogenation steps, whereas the strong acid sites provided by the zeolite create carbonium ions. These metallic and acid sites require an optimum balance to provide maximum isomerization efficiency, while deviation from the optimum balance will seriously affect both isomerization and hydrocracking reactions. However, when the acid sites density and strength overcompensate for the balancing effectiveness of metal sites, enhanced hydrocracking, which is a traditional competitor of hydroisomerization, is expected which may become excessive and cause feed loss [11]. Hydrocracking may take place if during the formation of an isomeric carbonium ion, the ion ruptures (hydrocracks) before it acquires a hydride ion to form a stable isoalkane molecule. This happens if the acidity strength of the catalyst and/or the temperature of reaction are high, because both isomerization and cracking reactions take place by the same mechanism (carbonium ion mechanism) [14].

Fig. 6 presents the effect of temperature on total n-paraffins conversion. Supporting Pt on ZSM-5 leads to the synthesis of the most active catalytic material (highest conversion), followed by mordenite and beta zeolite supported catalysts. As previously discussed Pt/ZSM-5 possesses the highest density and strength of acid sites, thus the difference in reactivity can be understood as the result of this different acid strength. More particularly, we can suggest that strong acid sites decrease the activation energy of the rate-limiting step and increase the conversion activity [39]. The inferior performance of mordenite, despite the fact that it exhibits similar acidic properties with ZSM-5, is an issue, which may be tentatively influenced by steric hindrance phenomena that hamper the accessibility of the reaction intermediates to acid sites as previously reported in the literature [40–42]. The slower diffusion of larger molecules is not somehow always a handicap, as it can be more effective for contacting the n-alkane molecules with the largest possible number of active sites as the one present in the sinusoidal channels of ZSM-5. Furthermore, the pores of ZSM-5 are of tridirectional structure, whereas MOR acquires a unidirectional channel structure [14]. For mordenite catalysts, conversion and selectivity are reported to be controlled more by the diffusional rates inside the pore structure rather than the acid/metallic site balance, while noble metal content does not modify their activity [42]. This agrees well with our results, according to which although Pt/MOR catalyst has the highest actual loading of Pt metal and similar acidity of Pt/ZSM-5, it presents lower activity than Pt/ZSM-5. Still, attributing the lower activity of Pt/MOR compared to Pt/ZSM-5 to the effect

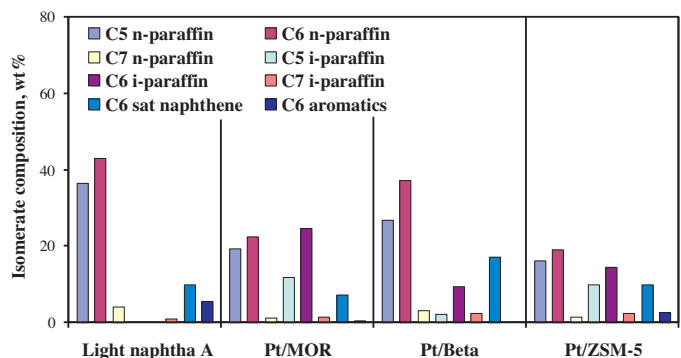


**Fig. 7.** Composition of isomerate product at  $280\text{ }^\circ\text{C}$  using as feed surrogate light naphtha A (reaction conditions:  $P=30$  bar,  $WHSV=2\text{ h}^{-1}$ ).

of the window size of the zeolite could be disputable as MOR is a large-pore zeolite with a ring major chemical size of 12, whereas ZSM-5 is a medium-pore zeolite with a 10-membered ring. However, with the straight channel of the ZSM-5 zeolite, diffusion is five times faster than in its sinusoidal channel for molecules close in size to the diameter of the pores; i.e. benzene.

The composition of the isomerate product, illustrated in Fig. 7, indicates that over all Pt/zeolite catalysts naphtha is selectively isomerized to  $C_5$ – $C_7$  isoparaffins, without formation of additional naphthenes or aromatics. Especially for the latter, it can be observed that almost total conversion of the feed aromatics is achieved over all three samples.

Fig. 8 presents the selectivity to  $C_5$ ,  $C_6$  and  $C_7$  isoparaffins as a function of conversion for the three Pt zeolite-supported catalysts. Although the data points were obtained at different temperatures, selectivity during isomerization of alkanes is widely accepted to depend essentially on the conversion level obtained, whichever the reaction temperature [20], while each zeolite is expected to exhibit a special selectivity in this process [38]. As shown in the figure, the increase of conversion (and subsequently temperature) favors the selective isomerization of paraffins mainly to  $C_5$  and  $C_6$  isoparaffins, while the production of  $C_7$  isoparaffins occurs at lower conversion levels and temperatures. The formation of  $C_6$  isomers exhibits a different behavior depending on zeolite support. The increase of conversion strongly favors  $C_6$  production on the Pt/BETA catalyst and Pt/MOR. Over Pt/ZSM-5, iso-hexanes increase gradually with temperature to reach a maximum of 60% selectivity at  $\sim 40\%$  conversion and then decrease gradually to 50% with further increase of conversion (80%). This gradual increase and decrease of isomers with temperature can be attributed to the different acid site strength of the ZSM-5 component as compared with the other (MOR and BETA) zeolite supports [14].

Since the reaction is equilibrium-limited, low temperature favors high concentrations of branched isomers, while enhanced cracking is expected at higher reaction temperatures [42]. Cracking activity can be estimated from the amount of light gases ( $C_1$ – $C_6$ ) in the gaseous exit stream of the reactor, presented in Fig. 9 as a function of reaction temperature for the three Pt/zeolite catalysts. Selectivity presents a slight decrease with temperature, as expected, especially in the case of Pt/ZSM-5, where a significant increase in the production of light gases is evidenced at high temperature, associated with secondary cracking reactions. It should be noted at this point that the concentration of light hydrocarbons in the gaseous stream exhibits the same trend also as a function of conversion level (not shown), with Pt/ZSM-5 exhibiting a much higher production of light gases than Pt/MOR and Pt/BETA.

The larger extent of hydrocracking reactions on Pt/ZSM-5 is additionally evidenced by the higher coke measured (7.2 wt% C) after reaction, as compared with the corresponding values of

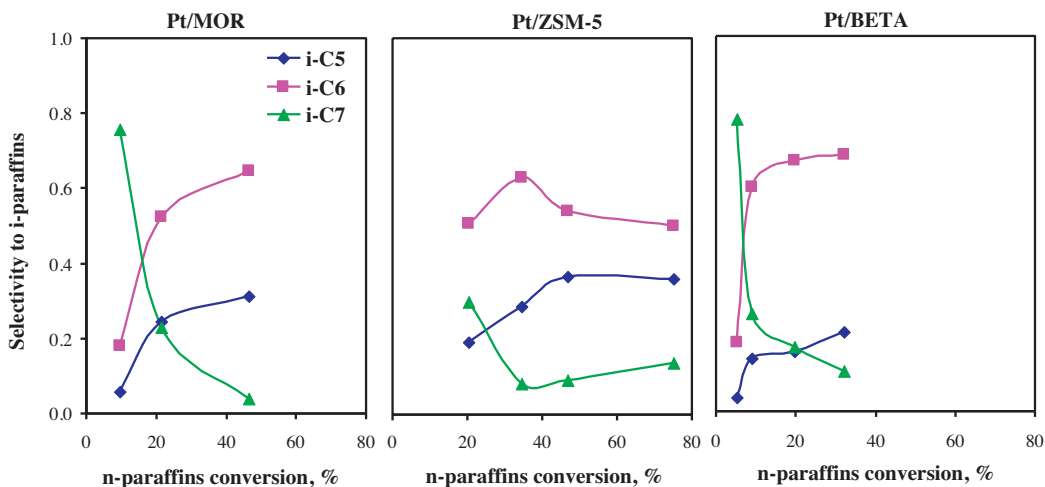


Fig. 8. Selectivity to iso-paraffins as a function of conversion using as feed surrogate light naphtha A (reaction conditions:  $P=30$  bar,  $WHSV=2\text{ h}^{-1}$ ).

3.3 wt% and 5.4 wt% for Pt/MOR and Pt/BETA, respectively. The lowest activity of Pt/BETA in combination with the second highest coke level formed during hydroisomerization experiments can be explained as follows: The large channels of BETA zeolite, together with the small size of the Pt crystallites (as evidenced by TEM analysis), allow a very rapid diffusion of the reactants. The moderate acidity of this zeolite, which is expected to limit cracking cannot be overlooked. However, the reaction intermediates are probably blocked inside the porosity of these zeolites where they can undergo, via successive carbocations, several reactions on the protonic sites: isomerization into monobranched isomers, then into very reactive multibranched isomers, which tend to crack rapidly, finally leading to high coke formation [27].

As the goal of the upgrading process is the mild reduction of the feed's cetane number, the cetane index of the isomerate product compared to that of the light feed A versus temperature for all catalysts is shown in Fig. 10. It is clear that hydroisomerization is a suitable process for upgrading BtL naphtha, since a lower cetane index is achieved, which decreases further with increasing temperature. The superiority of Pt/ZSM-5 is once more evident, as it can achieve the desired mild cetane index reduction at low temperatures.

### 3.2.2. Effect of naphtha feed

In view of these results, the catalytic performance of the most active material, Pt/ZSM-5, was also tested for the

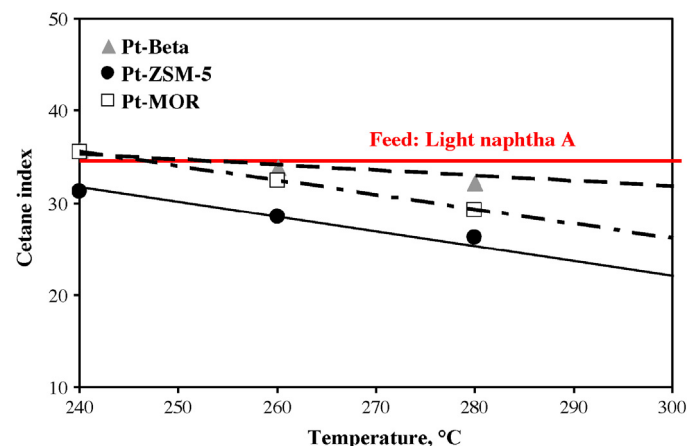


Fig. 10. Cetane index (CI) as a function of reaction temperature using as feed surrogate light naphtha A (reaction conditions:  $P=30$  bar,  $WHSV=2\text{ h}^{-1}$ ).

hydroisomerization of the heavier model naphtha B. The conversion of total n-paraffins for both feeds as a function of reaction temperature is presented in Fig. 11. It can be seen that the Pt/ZSM-5 catalyst is also active toward the isomerization of heavier normal paraffins as the conversion of the heavier naphtha is higher than that of the lighter, especially as temperature increases. Of course,

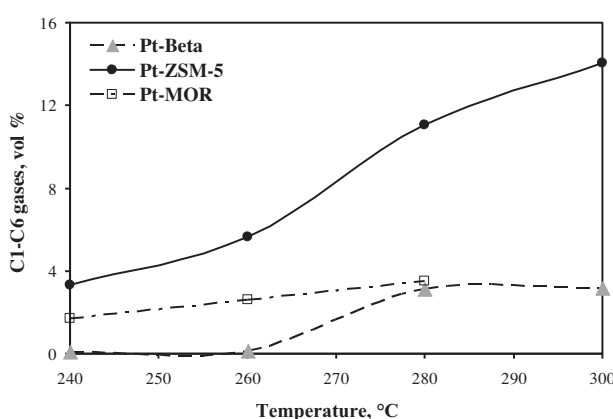


Fig. 9. Concentration of light gases as a function of reaction temperature using as feed surrogate light naphtha A (reaction conditions:  $P=30$  bar,  $WHSV=2\text{ h}^{-1}$ ).

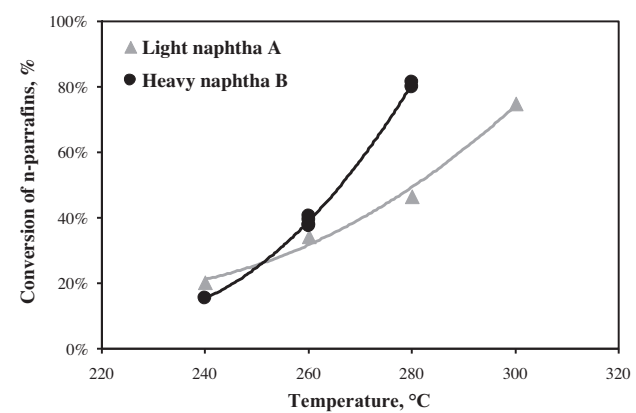


Fig. 11. Conversion of n-paraffins as a function of reaction temperature for light naphtha A and heavy naphtha B over Pt/ZSM-5 catalyst (reaction conditions:  $P=30$  bar,  $WHSV=2\text{ h}^{-1}$ ).

selectivity is very important in this case, as the goal of the study is the development of catalysts with satisfactory isomerization activity for heavier hydrocarbons, while preventing secondary cracking reactions to lighter products and gases.

Fig. 12 shows the composition of the isomerate product over Pt/ZSM-5 at constant reaction temperature (260 °C) for both heavy and light naphtha feeds. The reaction temperature was selected to be 260 °C as the conversion levels at this temperature are similar for both feeds. A careful inspection of the isomerate composition indicates that with the light feed a good selectivity is attained, as also discussed in the previous paragraph, as both pentane and hexane in the feed are isomerized to isopentane and methyl-pentane, respectively. The concentration of C<sub>4</sub> and lighter hydrocarbons in the product, indicative of cracking activity, is rather low (not shown). In the case of the heavier feed, the catalyst seems to preferentially isomerize C<sub>7</sub> up to C<sub>10</sub> normal alkanes to iso-octane (C<sub>8</sub> isoparaffin). The concentration of light alkanes is again low, confirming that Pt/ZSM-5 is able to successfully isomerize heavier hydrocarbons with limited cracking side reactions at the investigated temperature range.

## 4. Discussion

### 4.1. Effect of zeolite structure

The very low Pt content in the catalysts investigated in our study suggests that the zeolitic component possesses a significant influence [14]. At this point, it should be probably additionally mentioned that unloaded catalytic materials (in absence of metals) such as ZSM-5 and MOR zeolites have been also tested by other groups as hydroisomerization catalysts. Aboul-Gheit et al. [44] found that unloaded alumina and MOR zeolite possess as catalysts [45] self-hydrogenating capability. Kanai et al. [46] showed that Brönsted acid sites become active hydrogenation sites of alkenes at higher temperatures. Furthermore, Chu et al. [47] stated that in the absence of active metal the acid centers of H-BEA zeolites themselves have hydrogenation–dehydrogenation activities [14].

Under the reaction conditions investigated in the present study, the structure of the zeolites was found to play a significant role, even equally important with acidity, as catalysts with similar acidic properties (Pt/MOR and Pt/ZSM-5) exhibited differentiating behavior. A faster mobility of the carbocation intermediate through more open and/or interconnected structures could explain this result [6]. The smallest pore size in ZSM-5 is about 5.1 Å, and can be compared to the effective kinetic diameter of iso-pentanes or iso-pentane (~5 Å). Thus, the restricted diffusion of i-C<sub>5</sub> in the pores would allow the molecule to be transformed on the acid sites to C<sub>1</sub>–C<sub>4</sub> products (mainly C<sub>3</sub> and C<sub>4</sub>). Moreover, the ZSM-5 contains not only a straight 10-ring channel system but also a zigzag 10-ring channel system. Slower migration of the intermediates within the zigzag 10-ring channel may lead to longer life-time of the intermediates [48], leading to an enhanced hydrocracking selectivity as observed in our case. On the other hand, in the small channels of ZSM-5, formation of multibranched alkylcarbenium ions that are most susceptible to cracking is suppressed due to steric or geometric constraints. So the enhanced hydrocracking selectivity over Pt/ZSM-5 at higher temperature and conversion levels can be probably attributed to the longer lifetime of the intermediates rather than to the formation of multibranched alkylcarbenium ions [39]. Preferential isomerization on the monodimensional molecular sieves regardless of acid strength, such as SAPO-11, -31, -41, ZSM-22 and -23 has been also reported [39]. Nevertheless, the conversion activity of higher alkanes (e.g. n-octane) is reported to depend on the acidity of molecular sieves. Both more acid sites and stronger acid sites increase the conversion of n-octane, explaining

better performance of the Pt/ZSM-5 catalyst when using the heavier naphtha feed [39].

Mordenite, a member of the large pore zeolites family, with a similar pore diameter as BEA zeolite (~7 Å), is generally considered a one-dimensional pore system, inducing single-file diffusion (SDF) [49]. SDF is the exclusion of the mutual passage of diffusants in zeolites with one-dimensional channels, which leads to patterns of molecular transportation which are different than normal diffusion occurring in zeolites with multi-dimensional pore networks [50]. Thus, the olefin intermediary can also have enough time to be transformed to C<sub>1</sub>–C<sub>4</sub> products (mainly C<sub>3</sub> and C<sub>4</sub>), as in ZSM-5. Interestingly the mordenite is reported as an unselective support, a behavior ascribed to the side pockets it possesses, delaying diffusion of the reaction products and favoring their cracking [51,52]. This is accordance with the general trend observed in our study, as the Pt/MOR catalyst exhibited the highest selectivity to smaller C<sub>5</sub> isomers (~80% selectivity at 40% conversion) and limited formation of C<sub>6</sub> and C<sub>7</sub> isoparaffins.

On the contrary, in beta zeolites with large-pore and tri-dimensional pore system, the iso-pentenes formed can be hydrogenated over metal sites to iso-pentane more easily, and diffusion of iso-pentene from the interior of the zeolite toward the external surface is faster, with an expected net result of a higher selectivity to iso-pentane. This was not the case for our significantly less acidic BETA zeolite, suggesting that both structure and acidic properties should be considered when interpreting isomerization results.

### 4.2. Effect of acidity

Whereas selectivity of isoparaffins depends primarily on the balance between metal and acid functions [2], catalyst acidity has a major influence on the hydroisomerization and hydrocracking yields. The acid site density and acid strength distribution are both important and the proper balance of these variables is critical in determining the reactivity and selectivity of the bifunctional catalysts. The number of acid sites in the 0.1% Pt/ZSM-5 catalyst is somehow larger than in 0.1% Pt/MOR, while the strength of acid sites in the latter is also slightly higher than in the former catalyst (Table 4). It seems that hydroisomerization activity is attributed to acquiring a large number of moderately strong acid sites, strong enough for carbonium ions suitable for stable branching of the n-paraffin. These acid sites, however, are either not so strong that the isomerized carbonium ion does not crack or especially for the Pt/ZSM-5 not further accessible for the branched susceptible to cracking products [14]. The same MOR(20) catalyst with the one used in our study is also reported to possess a significant number of sites of weak, medium and strong acidity but its activity drops rapidly through strong deactivation [38]. Thus, because coking increases with increasing cracking rate, the low conversion exhibited by catalyst Pt/MOR(20) arises from strong deactivation immediately after the reaction starts through deposition of coke in the one-dimensional channel network of the zeolite [38]. This could be an explanation for the reduced activity of the Pt/BETA zeolite. Finally, the extremely low activity of the Pt/BETA zeolite is more straightforwardly explained on the basis that this catalyst exhibits a significantly lower concentration of acid sites.

### 4.3. Effect of Pt morphology and dispersion

In addition to the acidity and porosity characteristics, highly dispersed Pt is expected to favor hydrogenation rather than hydrocracking pathways. Testing Pt/H-Y and Pt/Al-MCM-41 showed that even if they both have weak acid sites and high surface area, Pt/Al-MCM-41 exhibited higher isomerization selectivity due to its higher Pt dispersion [19]. Although Pt dispersion could not be

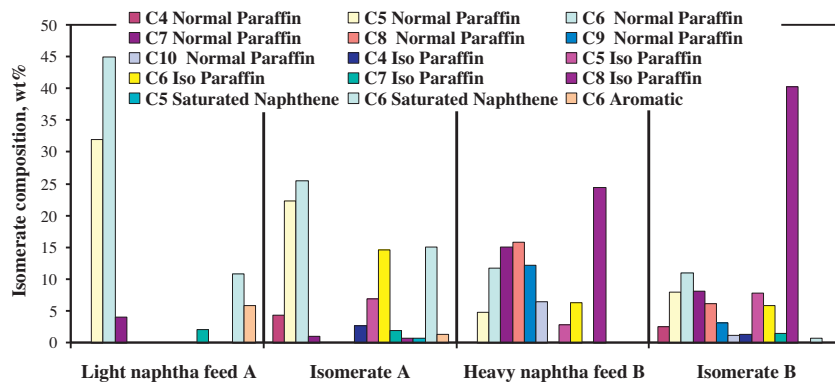


Fig. 12. Composition of isomerate product at 260 °C for light naphtha A and heavy naphtha B over Pt/ZSM-5 catalyst (reaction conditions:  $P = 30$  bar, WHSV = 2 h<sup>-1</sup>).

measured by H<sub>2</sub>-TPR for our samples due to the extremely low Pt content, this was compensated by the extensive TEM characterization of the investigated Pt/zeolite catalysts.

The Pt/ZSM-5 material exhibited the highest crystallinity and specific morphology for the Pt nanoparticles. HRTEM experiments coupled with EDS analysis revealed that the Pt particles are homogeneously dispersed onto the zeolite surface and maintain their cubic shape, constant sizes and surface and bulk chemical purity. In addition, an even distribution of the Pt ions inside the ZSM-5 framework can be assumed, as has been previously shown [11,53] for such materials prepared via metal impregnation, due to the medium pore sizes of the ZSM-5 zeolite. On the other hand, Pt/mordenite catalysts exhibit larger pore sizes that do not facilitate the homogeneous distribution of Pt ions inside the zeolite matrix. The vast majority of Pt particles was detected almost exclusively onto the surface of mordenite platelets and exhibited inferior crystalline, morphological and chemical features compared to these of the Pt/ZSM-5 material. This is in accordance to literature [53], where it has been reported that the dispersion of platinum on Pt/ZSM-5 catalysts is higher than on corresponding Pt/MOR catalysts, leading to higher activity. Therefore the higher overall activity in n-paraffins conversion measured over Pt/ZSM-5 in this study could be related also to the higher Pt dispersion. However, Pt/MOR exhibited higher selectivity and lower hydrocracking activity. The less even distribution of Pt that seems to occur in the channels of MOR zeolite compared to ZSM-5 [53] could have also resulted in some diffusion restriction and caused the obvious decrease of the rate of hydrocracking particularly at higher temperatures. It is well known that the effect of diffusion appears at higher reaction temperatures because the increase of the chemical reaction with temperature is much faster than the rate of diffusion, therefore rendering diffusion the rate controlling phenomenon [11].

The Pt/BETA zeolite catalyst exhibited no discrete Pt nanoparticle formation. Without overlooking its reduced acidity, this may also explain its inferior performance, as Pt needs to be in both morphologies – nanoparticle and regularly distributed into the zeolite matrix [54] – since the former morphology possesses high activity in olefin hydrogenation, hence suppressing catalyst deactivation by coke formation. Indeed, in order to have an active and, at the same time not deactivating catalyst, the combination of Pt distinct nanoparticles with high dehydrogenation activity and platinum hydride/Brønsted acid pair sites is required. Moreover, even though good metal dispersion, determined by H<sub>2</sub> chemisorption, has been reported for Pt/BETA catalysts [38], beta zeolites contain more defects and terminal silanol groups which stabilize Pt species in a more oxidized state and render their reduction more difficult. The latter is also in accordance with the residual Cl content detected by EDS in the Pt/BETA zeolite. Thus, insufficient performance of Pt/BETA zeolite can also be related to the presence of unreduced

Pt species, which are inactive toward the dehydrogenation of the hydrocarbons to the olefinic intermediates.

It seems that Pt/ZSM-5 catalyst is superior because, among others, Pt in ZSM-5 is both into discrete nanoparticle morphology and into the ZSM-5 lattice sites, in contrary to the mordenite (presenting, as anticipated, mainly nanoparticles onto the zeolite surface) and beta (mainly highly dispersed Pt as expected, which might be though difficult to reduce). Combination of discrete particles and metal dispersed into the zeolite matrix as observed in Pt/ZSM-5 is required for good catalytic performance toward isomerization possibly via i.e. a synergy effect [54]. In previous studies [54], the combination of both morphologies for Pt was accomplished only for relatively high loadings (2.6 wt%), which is drawback considering catalyst preparation costs. The results in our study proved that discrete Pt particle formation with superior structural characteristics takes place even for quite low Pt loadings (~0.1 wt%), thus presenting a highly active and selective system for alkane hydroisomerization. In that way, a remarkable reduction of the catalyst preparation costs is manifested, compared to systems examined in the literature so far.

In conclusion the superior catalytic performance of the Pt/ZSM-5 material is merely a combination of the existence of strong acid sites onto the zeolite matrix and their interaction with the specific morphology platinum species present on the surface and into the bulk of the zeolite. As has been previously discussed [54], the most active hydroconversion sites of the catalyst are not bi-functional in the sense of the classical mechanism; that is, the metallic and the acidic functions cannot be separated. The Pt sites were described as atomic Pt<sup>0</sup> or small metal particles in interaction with adjacent Brønsted acid hydroxyl groups. The platinum particles were assumed to assist the acid sites in generating carbenium ions. The Pt and H<sub>2</sub> were suggested to cooperate in providing hydride ions to neutralize the carbenium ions facilitating product release and protons to balance negative charge on the zeolite framework.

## 5. Conclusions

A systematic study of the effect of the zeolite support (mordenite, ZSM-5, and beta zeolite) on the activity and selectivity of low loading Pt catalysts in naphtha hydroisomerization is presented. All Pt/zeolite catalysts were found effective in isomerizing naphtha selectively to C<sub>5</sub>–C<sub>7</sub> isoparaffins, without formation of additional naphthenes or aromatics, under the investigated reaction conditions. The selective isomerization of paraffins to C<sub>5</sub> and C<sub>6</sub> isoparaffins was favored at high reaction temperature, while the production of C<sub>7</sub> isoparaffins occurred at lower temperature (and therefore lower conversion). Calculation of the cetane index of the isomerates clearly showed a decrease of the CI of the feed after hydroisomerization, with a decreasing trend as temperature is

increased. Pt/ZSM-5 catalyst was also active toward the isomerization of heavier normal paraffins, like BtL naphtha, as demonstrated by experiments with heavier naphtha feed. In this case, the catalyst preferentially isomerized C<sub>7</sub> up to C<sub>10</sub> normal alkanes to iso-octane (C<sub>8</sub> isoparaffin).

Supporting Pt on ZSM-5 led to the synthesis of the most active catalytic material (highest conversion), followed by mordenite and beta zeolite supported catalysts. As Pt/ZSM-5 possesses the highest density and strength of acid sites, the difference in reactivity can be understood as the result of this different acid strength. The inferior performance of mordenite, despite the fact that it exhibits similar acidic properties with ZSM-5, is possibly a result of steric hindrance phenomena that hamper the accessibility of the reaction intermediates. The structure of the zeolites seems to play a significant role, even equally important with acidity. A faster mobility of the carbocation intermediate through more open and especially interconnected structures could explain the differences between the performance of Pt/MOR and Pt/ZSM-5. The superior activity of Pt/ZSM-5 is however associated with enhanced production of dry gases at high temperature, associated with secondary cracking reactions. This enhanced hydrocracking selectivity could be due to the slower migration of the intermediates within the zigzag 10-ring channel of ZSM-5, which may lead to longer life-time of the intermediates and subsequently cracking reactions.

The overall superiority of Pt/ZSM-5 catalyst is attributed among others, to Pt presence in ZSM-5 as *both* discrete nanoparticle morphology and into the ZSM-5 lattice sites, in contrary to the mordenite (presenting, as anticipated, mainly nanoparticles onto the zeolite surface) and beta (mainly highly dispersed Pt as expected, which might be though difficult to reduce). Combination of discrete particles and metal dispersed into the zeolite matrix as observed in Pt/ZSM-5 is required for good catalytic performance toward isomerization possibly via i.e. a synergy effect.

## Acknowledgement

The work was conducted with support from the EU under the frame of the FP7 funded OPTFUEL ("Optimized Fuels for Sustainable Transport project") – Grant Agreement No.: 218890.

## Appendix A. Supplementary data

Supplementary data associated with this article can be found, in the online version, at <http://dx.doi.org/10.1016/j.apcatb.2013.03.026>.

## References

- [1] RENEW Project final report, 2008, [www.renew-fuel.com](http://www.renew-fuel.com)
- [2] H. Deldari, *Applied Catalysis A* 293 (2005) 1–10.
- [3] Z.B. Wang, A. Kamo, T. Yoneda, T. Komatsu, T. Yashima, *Applied Catalysis A* 159 (1997) 119–132.
- [4] M. Belloum, C. Travers, J.P. Bourronville, *Revue de l'Institut Français du Pétrole* 46 (1991) 89–107.
- [5] M. Guisnet, F. Alvarez, G. Giannetto, G. Perot, *Catalysis Today* 1 (1987) 415–433.
- [6] C.M. López, V. Sazo, P. Pérez, L.V. García, *Applied Catalysis A* 372 (2010) 108–113.
- [7] L.W. Lin, F.L. Zhang, *Bulletin of Institute of Chemical Physics of the Chinese Academy of Sciences. Book 1*, Science Press, Beijing, 1964.
- [8] L.W. Lin, D.B. Liang, G.Y. Cai, F.L. Zhang, *Journal of Fuel Chemistry and Technology* 6 (1965) 55–63.
- [9] B.N. Jiang, L.W. Lin, F.L. Zhou, I.V. Kalechits, *Petroleum Processing* 2 (1958) 6–13.
- [10] S. Rasev, *Thermal, Catalytic Processes in Petroleum Refining*, Marcel Dekker, Inc., New York, Basel, 2003.
- [11] A.K. Aboul-Gheit, S.M. Abdel-Hamid, D.S. El-Desouki, *Petroleum Science and Technology* 29 (2011) 2346–2360.
- [12] H. Weyda, F. Köhler, *Catalysis Today* 81 (2003) 51–55.
- [13] M.J. Ramos, A. Lucas, V. Jiménez, P. Sánchez, J.L. Valverde, *Fuel Processing Technology* 89 (2008) 721–727.
- [14] A.K. Aboul-Gheit, S.M. Abdel-Hamid, D.S. El-Desouki, *Petroleum Science and Technology* 28 (2010) 582–593.
- [15] P. Liu, X. Zhang, Y. Yao, J. Wang, *Reaction Kinetics, Mechanisms and Catalysis* 1 (2010) 217–226.
- [16] A.K. Aboul-Gheit, A.P. Awadallah, N.A.K. Aboul-Gheit, E.A. Solyman, M.A. Abdel-Aaty, *Applied Catalysis A* 334 (2008) 304–310.
- [17] R. Parton, L. Uytterhoeven, J.A. Martens, P.A. Jacobs, G.F. Froment, *Applied Catalysis A* 76 (1991) 131–142.
- [18] P. Mériadeau, V.A. Tuan, F. Lefebvre, V.T. Nghiem, C. Naccache, *Microporous and Mesoporous Materials* 22 (1998) 435–449.
- [19] K.-C. Park, S.-K. Ihm, *Applied Catalysis A* 203 (2000) 201–209.
- [20] A. Chica, A. Corma, *Journal of Catalysis* 187 (1999) 167–176.
- [21] A. Voorhies, P.A. Bryant, *AIChE Journal* 14 (1968) 852–856.
- [22] K.J. Chao, H.C. Wu, L.J. Leu, *Applied Catalysis A* 143 (1996) 223–243.
- [23] F. Alvarez, F.R. Ribeiro, G. Perot, C. Thomazeau, M. Guisnet, *Journal of Catalysis* 162 (1996) 179–189.
- [24] Z.B. Wang, A. Kamo, T. Yoneda, T. Komatsu, T. Yashima, *Applied Catalysis A: General* 159 (1997) 119–132.
- [25] M. Hochtl, A. Jentys, H. Vinek, *Journal of Catalysis* 190 (2000) 419–432.
- [26] M.C. Claude, G. Vanbutsele, J.A. Martens, *Journal of Catalysis* 203 (2001) 213–231.
- [27] A. Soualah, J.L. Lemberton, L. Pinard, M. Chater, P. Magnoux, K. Moljord, *Applied Catalysis A* 336 (2008) 23–28.
- [28] A. de Lucas, P. Sánchez, F. Dorado, M.J. Ramos, J.L. Valverde, *Applied Catalysis A* 294 (2005) 215–225.
- [29] A.K. Aboul-Gheit, S.A. Ghoneim, A.A. Al-Owais, *Applied Catalysis A* 170 (1998) 277–283.
- [30] A.K. Aboul-Gheit, S.M. Abdel-Hamid, A.E. Awadallah, *Oil Gas: European Magazine* 30 (2004) 40–44.
- [31] A.K. Aboul-Gheit, N.A.K. Aboul-Gheit, Erdol, Erdgas, Kohle 119 (2003) 28–34.
- [32] A. Patriceon, E. Benazzi, Ch Travers, J.Y. Bernhard, *Catalysis Today* 65 (2001) 149–155.
- [33] B. Modhera, M. Chakraborty, H.C. Bajaj, P.A. Parikh, *Reaction Kinetics, Mechanisms and Catalysis* 99 (2010) 421–429.
- [34] T. Yashima, Z.B. Wang, A. Kamo, T. Yoneda, T. Komatsu, *Catalysis Today* 29 (1996) 279–283.
- [35] J.F. Allain, R. Magnoux, Ph Schulz, M. Guisnet, *Applied Catalysis A* 152 (1997) 221–235.
- [36] B.V. Sousa, K.D. Brito, J.J.N. Alves, M.G.F. Rodrigues, C.M.N. Yoshioka, D. Cardoso, *Reaction Kinetics, Mechanisms and Catalysis* 102 (2011) 473–485.
- [37] C. Baerlocher, W.M. Meier, D.H. Olson, *Atlas of Zeolite Framework Types*, fifth revised ed., Elsevier, Amsterdam, 2001.
- [38] C. Jiménez, F.J. Romero, R. Roldán, J.M. Marinas, J.P. Gómez, *Applied Catalysis A* 249 (2003) 175–185.
- [39] H. Yunfeng, W. Xiangsheng, G. Xinwen, L. Silue, H. Sheng, S. Haibo, B. Liang, *Catalysis Letters* 100 (2005) 59–65.
- [40] G. Kinger, H. Vinek, *Applied Catalysis A* 218 (2001) 139–149.
- [41] M.A. Makarova, A.E. Wilson, B.J. van Liempt, C.M.A.M. Mesters, A.W. de Winter, C. Williams, *Journal of Catalysis* 175 (1997) 170–177.
- [42] A. Brito, F.J. García, M.C. Alvarez-Galvá, M.E. Borges, C. Díaz, V.A. de la Peña O'Shea, *Catalysis Communications* 8 (2007) 2081–2086.
- [43] A.K. Aboul-Gheit, M.F. Menoufy, A.M. El-Fadly, O.I. Sif-El-Din, S.A. Sultan, *Journal of Chemical Technology and Biotechnology* 32 (1982) 1000–1006.
- [44] A.K. Aboul-Gheit, M.F. Menoufy, A.K. El-Morsy, S.M. Abdel-Hamid, *Zeolites* 7 (1987) 353–359.
- [45] J. Kanai, J.A. Martens, P.A. Jacobs, *Journal of Catalysis* 133 (1992) 527–543.
- [46] J.Y. Chu, M.P. Rosynek, J.H. Lunsford, *Journal of Catalysis* 178 (1998) 352–362.
- [47] J.A. Martens, P.A. Jacobs, *Zeolites* 6 (1986) 334–348.
- [48] G. Lei, B. Carvill, W. Sachtler, *Applied Catalysis A* 142 (1996) 347–359.
- [49] J. Kärger, *Molecular Sieves* 7 (2008) 329–366.
- [50] A. Chica, A. Corma, P.J. Miguel, *Catalysis Today* 65 (2001) 101–110.
- [51] J.-K. Lee, H.-K. Rhee, *Catalysis Today* 38 (1997) 235–242.
- [52] A.K. Aboul-Gheit, A.E. Awadallah, D.S. El-Desouki, N.A.K. Aboul-Gheit, *Petroleum Science and Technology* 27 (2009) 2085–2096.
- [53] F. Lonyi, A. Kovacs, A. Szegedi, J. Valyon, *Journal of Physical Chemistry C* 113 (2009) 10527–10540.